# **CONFERENCE PRE-PRINT**

# CLUSTER DYNAMICS MODELING OF DEFECT EVOLUTION IN NEUTRON-IRRADIATED TUNGSTEN FOR FUSION APPLICATIONS

Z.F. WANG, C. YIN\*, Z. LIU, Z. CHEN, S.F. MAO, M.Y. YE\* University of Science and Technology of China Hefei, China Email: chaoyin@ustc.edu.cn; yemy@ustc.edu.cn

#### **Abstract**

Tungsten (W) is considered the most promising plasma-facing material, which can be exposed to high neutron loads at high temperature. However, a significant number of defects, such as dislocation loops, voids, and precipitates, are generated in W under neutron irradiation, leading to the degradation of its material properties. This study employed a cluster dynamics model that incorporates the one-dimensional migration of dislocation loops to simulate defect evolution in single-crystal and polycrystalline W under neutron irradiation at 600–1200 °C, and compared the results with experimental data obtained from the BR2 reactor. A general agreement with experimental results was achieved, and the underlying causes of the observed discrepancies were analysed.

#### 1. INTRODUCTION

In magnetic confinement nuclear fusion devices, Tungsten (W) is considered the most promising plasma-facing material (PFM) [1], which will be exposed to high neutron loads at high temperatures [2] (up to 1200 °C for divertor during steady-state operation). Such an extreme environment leads to the production of point defects, dislocation loops, voids, and precipitates consisting of transmutation elements such as Rhenium (Re) and Osmium (Os) in W [3]. As is known to all, these defects will result in the degradation of mechanical properties and may reduce service lifetime [2–4]. Therefore, many studies were carried out to investigate the underlying mechanisms of the microstructural evolution of irradiation-induced defects [3, 5].

Due to the scarcity of fusion neutron sources, experimental studies often rely on fission neutron sources as alternatives [3]. Major facilities include mixed-spectrum reactors such as HFIR and BR2, as well as fast neutron reactors like JOYO, which differ primarily in their neutron energy spectra. Extensive neutron irradiation experiments have been conducted on both single-crystal and polycrystalline W at these facilities [6–16]. However, experimental approaches are often limited by high costs, lengthy timeframes, and an inherent inability to fully replicate the effects of fusion neutron irradiation. As a result, computational modelling has become an indispensable tool for investigating material behaviour under neutron irradiation. It is well recognized that such simulations are typically multi-scale in both time and space [5]. For mesoscale materials modelling, cluster dynamics (CD) and the kinetic Monte Carlo (KMC) method are usually widely employed to analyse the evolution of irradiation-induced defect features in W. Compared to KMC, the CD method holds an advantage in simulating the long-term evolution of large-scale defects due to constraints in computational resources. Li et al. [17] employed a CD model incorporating helium (He) atoms to investigate the accumulation and diffusion of He in W under both separate He implantation and synergistic irradiation with neutrons. Mannheim et al. [18] and Zhang et al. [19] calculated the concentration of point defect clusters under the assumption that only small clusters are mobile, thereby investigating the phenomenon of irradiation-induced recrystallization in W. Dunn et al. [20] developed a spatially resolved stochastic cluster dynamics (SRSCD) method to study the problem of He desorption in thin iron foils. Mohamed et al. [21] simulated and compared the defect evolution behaviour in W at temperatures up to 600 °C, based on experimental results from the BR2 reactor. Their model incorporated various clusters, including 1/2(111) and (100) dislocation loops, C15 clusters, as well as the high mobility of 1/2(111) dislocation loops. Although numerous simulation studies have modelled the evolution of irradiation-induced defects in W under neutron irradiation, several challenges remain. There is a lack of simulations capable of directly and accurately comparing complex defect evolution processes, along with insufficient consideration of the rapid migration behaviour of dislocation loops in W, and inadequate modelling of the evolution and effects of transmutation-induced precipitates.

The present study employs a CD model that incorporates the rapid one-dimensional migration of dislocation loops and clusters with sizes exceeding 10 nm. Simulations were performed for both single-crystal and polycrystalline W neutron irradiation experiments conducted in the BR2 reactor, covering a temperature range of 600–1200°C. The aim is to achieve close agreement with experimental results, thereby providing accurate defect information for subsequent predictions of other material properties.

### 2. CLUSTER DYNAMICS MODEL

CD, based on the rate theory, is a mesoscale approach used to model the evolution of defects in materials. It can describe the generation, diffusion, reaction, and growth of defect clusters, as well as their absorption at sinks like grain boundaries and dislocation lines. In our model, the mean-field approximation is adopted, implying that defect clusters are spatially uniformly distributed. This assumption allows the concentration of specific defects to represent corresponding cluster types. Consequently, the temporal evolution of cluster concentrations is described by a CD master equation—shown as Equation (1)—which includes source, reaction, and sink terms,

$$\frac{dC_x}{dt} = G_x + \sum_{(y,z)} (R_{y+z\to x} - R_{x\to y+z}) - \sum_{(y,z)} (R_{x+y\to z} - R_{z\to x+y}) + L_x , \qquad (1)$$

where C denotes the concentration of clusters, the subscript x indicates the type of cluster. Source term G represents the defect production rate. Reaction term R describes the interaction rate of different reactions, and L signifies the loss rate of the defects through sinks. The diffusion term has been omitted in the equation under the mean-field approximation.

#### 2.1. Source term

For the calculation of *G*, neutron spectra from various reactors were acquired and used as input to the "SPECTRA-PKA" code to compute the corresponding PKA spectra [22, 23]. The total number of Frenkel pairs was then determined based on molecular dynamics (MD) simulation results from Reference [24], which provided Frenkel pair production data for PKAs at different energies. In addition to a large number of point defects, defect clusters of larger sizes can also be directly generated via the cascade process, so a modified power-law distribution relationship from Reference [25] was employed here to describe this phenomenon.

$$G_{x} = \begin{cases} (1 - f_{\theta})G_{\text{tot}} & \text{for } x = 1 \\ A_{\theta} \left(\frac{1}{x} - \frac{1}{N_{c}}\right)^{S_{\theta}} & \text{for } 2 \le x \le N_{c} \\ 0 & \text{otherwise} \end{cases}$$
 (2)

Here, the variable  $\theta$  represents either a self-interstitial atom (I) or a vacancy (V).  $G_{tot}$  represents the total Frenkel pair production rate, and  $f_{\theta}$  ( $\theta = I$ , V) denotes the fraction thereof that forms clusters. The exponent  $S_{\theta}$  is a temperature-dependent exponent, and  $A_{\theta}$  represents pre-factors that can be determined from the total number of clustered defects.  $N_{c}$  represents the largest cluster size considered, with values of 1000 for interstitial clusters and 2000 for vacancy clusters, respectively[26, 27].

### 2.2. Reaction term

The reaction rates employed in this work are cited from Reference [20] wherein the reactions are categorized into two types: clustering reactions and dissociation reactions. The former refers to the aggregation of two clusters to form a new cluster, and the latter describes the dissociation of one cluster, resulting in the splitting into two clusters. In clustering reactions, at least one reactant must be a mobile cluster, and the corresponding reaction rate formulas differ depending on the types of migration. The present study assumes that mobile vacancy clusters and small SIA clusters (Size≤3) undergo three-dimensional (3D) migration, while larger interstitial clusters (Size≥4) exhibit one-dimensional (1D) migration. The dissociation reactions are limited to the emission of an interstitial or vacancy from interstitial clusters or the emission of a vacancy from vacancy clusters. Furthermore, we consider that the reaction rate R for both reactions is proportional to the concentration of the reactants, expressed as follows:

$$\begin{cases} R_{x+y\to z} = k_{x+y\to z}^+ C_x C_y \\ R_{z\to x+y} = k_{z\to x+y}^- C_z \end{cases}$$
 (3)

The specific reaction rate formulas and diffusion coefficients are presented separately in Table 1 and Table 2.

TABLE 1. THE REACTION RATES FOR ALL CONSIDERED REACTIONS[20]

Reaction	Reaction rate coefficient $k^+/k^-$	
Clustering reactions		
$V_x + V_y \rightarrow V_{x+y}$ ; $V_x + I_y \rightarrow V_{x-y}$ or $I_{y-x}$ (3D SIA)	$4\pi (r_x + r_y)(D_x + D_y)^*$	
$I_x + I_y \rightarrow I_{x+y} $ (3D + 3D SIA)	$4\pi Z_{\rm int} \left(r_x + r_y\right) \left(D_x + D_y\right)^{**}$	
$V_x + I_y \rightarrow V_{x-y}$ or $I_{y-x}$ (1D SIA)	$(4\pi r_x + 2\pi r_y)D_x + \pi^2(r_x + r_y)^4 D_y C_x$	
$I_x + I_y \rightarrow I_{x+y} $ (3D+1D SIA)	$Z_{\text{int}} \left( 4\pi r_x + 2\pi r_y \right) D_x + Z_{\text{int}}^4 \pi^2 \left( r_x + r_y \right)^4 D_y C_x$	
$I_x + I_y \rightarrow I_{x+y} \text{ (1D+1D SIA)}$	$Z_{\rm int}^4 \pi^2 \left(r_x + r_y\right)^4 \left(D_x C_y + D_y C_x\right)$	
Dissociation reactions		
$I_{x+1} \rightarrow I_x + I; V_{x+1} \rightarrow V_x + V; I_{x+1} \rightarrow I_{x+2} + V$	$\frac{k^+}{\Omega} \exp(\frac{-E_b^+}{k_B T})^{***}$	

<sup>\*</sup>r represents the cluster radius; D means the diffusion coefficient, following the Arrhenius law:  $D = D_0 \exp(-E_m / k_B T)$ , where  $D_0$  denotes the pre-exponential factor,  $E_{\rm m}$  represents the migration energy for diffusion,  $k_{\rm B}$  is the Boltzmann constant, and T is the temperature.

TABLE 2. MOBILITY PARAMETERS FOR INTERSTITIAL AND VACANCY DEFECTS [21]

Cluster	Pre-exponential factor(m <sup>2</sup> ·s <sup>-1</sup> )	Migration energy (eV)
$I_1(3D)$	$9.981 \times 10^{-11}$	0.165
$I_2(3D)$	$8.648 \times 10^{-10}$	0.222
$I_3(3D)$	$3.47 \times 10^{-10}$	0.203
$I_n, n \ge 4 (1D)$	$9.981 \times 10^{-11}/n^{0.5}$	0.1
$V_1(3D)$	$1.77 \times 10^{-6}$	1.66
$V_m, 4 \ge m \ge 2 (3D)$	$1.77 \times 10^{-6}$ /m	1.66
V <sub>m</sub> , m≥5 (immobile)	0	-

#### 2.3. Sink term

In our simulations, dislocation loops and grain boundaries are considered sinks for defects, exhibiting distinct sink strengths depending on the type of defect clusters. In this study, we assume that only point defects can be absorbed by these sinks, as interactions between defect clusters and grain boundary dislocations involve more complex behaviours that are consequently neglected in this model. The corresponding sink strengths are given in Equations (4) and (5) [28].

$$\begin{cases} k_{\rm DL,1D}^2 = 2(\pi(r_d + r_{\rm cluster})\rho_d)^2 \\ k_{\rm DL,3D}^2 = \frac{2\pi\rho_d(1 - \rho^2)}{-\ln(\rho) - 0.75 + 0.25\rho^2(4 - \rho^2)} \end{cases}, \tag{4}$$

<sup>\*\*</sup>  $Z_{\text{int}}$  is a constant reflecting the preference of interstitial clusters to absorb other interstitials, taken as  $Z_{\text{int}} = 1.2$  in this paper[17].

<sup>\*\*\*\*</sup>  $k^+$  is the coefficient of the corresponding clustering reactions;  $\Omega$  represents the atomic volume, which is equal to  $a_0^3/2$ , where  $a_0$  denotes the lattice constant.  $E_b$  represents the binding energy of the corresponding clustering reactions, cited from [17]

where  $\rho = (r_d + r_{\text{cluster}})\sqrt{\pi\rho_d}$ ,  $r_{\text{d}}$  denotes the dislocation capture radius and  $\rho_{\text{d}}$  represents the dislocation line density [29].

$$\begin{cases} k_{\rm GB,1D}^2 = 15 / R_{\rm GB}^2 \\ k_{\rm GB,3D}^2 = 14.4 / R_{\rm GB}^2 \end{cases}$$
(5)

where R<sub>GB</sub> means the average grain radius. Then the sink term can be derived from the sink strength by:

$$L_{\rm r} = k_{\rm r}^2 D_{\rm r} C_{\rm r} \,. \tag{6}$$

# 2.4. Numerical algorithm

Due to the stiff nature of the CD equations, this study employed the BDF (Backward Differentiation Formula) method from the CVODE package within the SUNDIALS (SUite of Nonlinear and DIfferential/ALgebraic equation Solvers) package, an open-source C language library developed by Lawrence Livermore National Laboratory, USA [30, 31].

# 3. RESULTS AND DISCUSSION

# 3.1. Single crystal simulation

We simulated the neutron irradiation experiment of single-crystal W at 600, 800, and 1200°C up to 0.2 dpa in the BR2 reactor [12], and obtained the relationship between defect concentration and irradiation dose as well as the defect size distribution after 0.2 dpa irradiation. To ensure a consistent and meaningful comparison with the experiment, all simulation results presented throughout this study pertain exclusively to visible clusters, defined as those larger than 0.5 nm. As shown in Fig. 1 and Fig. 2:

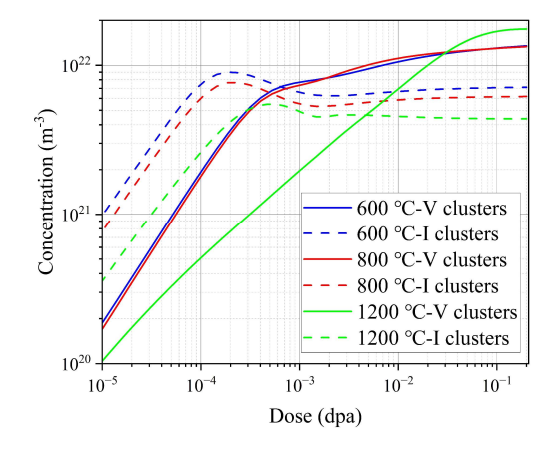


FIG. 1. The relationship between defect concentration and irradiation dose at 600°C, 800°C, and 1200°C. The solid curves represent V clusters. while the dashed curves denote I clusters.

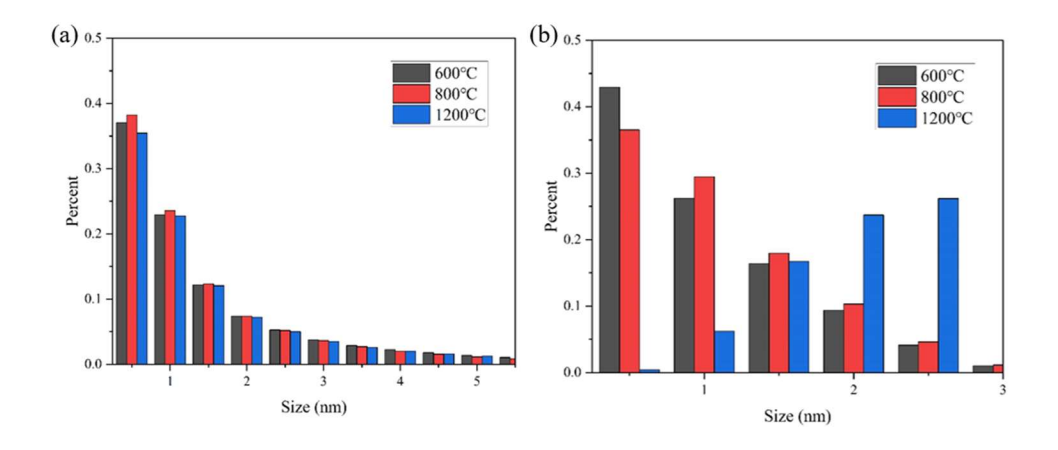


FIG. 2. The percentage size distribution of defect clusters after 0.2 dpa irradiation at 600 °C, 800 °C, and 1200 °C: (a) I clusters and (b) V clusters

As can be seen from Fig. 1, the total concentrations of both I and V clusters generally increase with rising irradiation dose, showing a tendency toward saturation beyond 0.1 dpa. The concentration of voids (V clusters) changes only slightly at 600 °C and 800 °C, but differs noticeably at 1200 °C, exceeding those at the other two temperatures in the dose range above 0.1 dpa. In contrast, the concentration of I clusters exhibits a consistent decreasing trend with increasing temperature.

Fig. 2 shows the percentage distribution of cluster sizes. For I clusters, the distributions exhibit minimal variation across temperatures, with smaller clusters in the 0.5~1 nm range accounting for a relatively high proportion—approximately 50%. V clusters demonstrate a similar distribution pattern at 600 °C and 800 °C. However, when the temperature rises to 1200 °C, significant cluster growth is observed, indicating enhanced mobility of V defects at this temperature, which substantially accelerates the coalescence of small clusters into voids.

Fig. 3 compares the simulation results with experimental data, focusing specifically on the average size and total concentration of defect clusters observed via transmission electron microscopy (TEM) characterization. As can be seen from the figure, the average cluster size shows good agreement with the experimental results, except for the I clusters at 1200 °C, where the simulated sizes are somewhat lower than the experimental values. The simulations generally underestimate the total concentration, though the discrepancy with the experimental data is within one order of magnitude. Moreover, while the concentration of voids increases with temperature, and that of I clusters decreases, a trend opposite to that seen in the experiments.

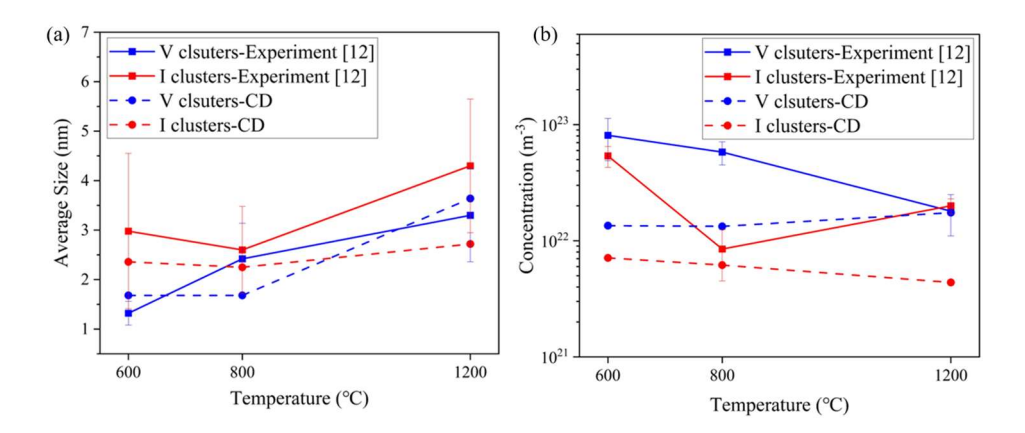


FIG. 3. The comparison between the experiment and simulation results for the average size and total concentration of visible clusters at 600 °C, 800 °C, and 1200 °C for single-crystal W. The solid line represents the experimental data, while the dashed line denotes the simulation results: (a) Average size and (b) total concentration.

### 3.2. Polycrystalline tungsten simulation

We also performed simulations of the neutron irradiation experiment on polycrystalline W at 900 °C with doses of 0.124, 0.183, 0.507, and 0.819 dpa for the BR2 reactor [9]. Similarly, a comparison was made between the simulation and experimental results regarding the average size and total concentration of visible defect evolution, as shown in Fig. 4. It was observed that the size of I clusters agrees well with the experimental results, showing an increasing trend with irradiation dose, although the growth rate is moderately slower than that observed experimentally. In contrast, the V clusters don't exhibit the same growth behaviour as seen in the experiments; instead, their sizes remained nearly constant at approximately 1.5 nm. The total concentration of defects in the simulation was consistently about one order of magnitude lower than the experimental values. It changed only gradually with increasing dose, whereas the experimental data showed a clear decreasing trend with dose.

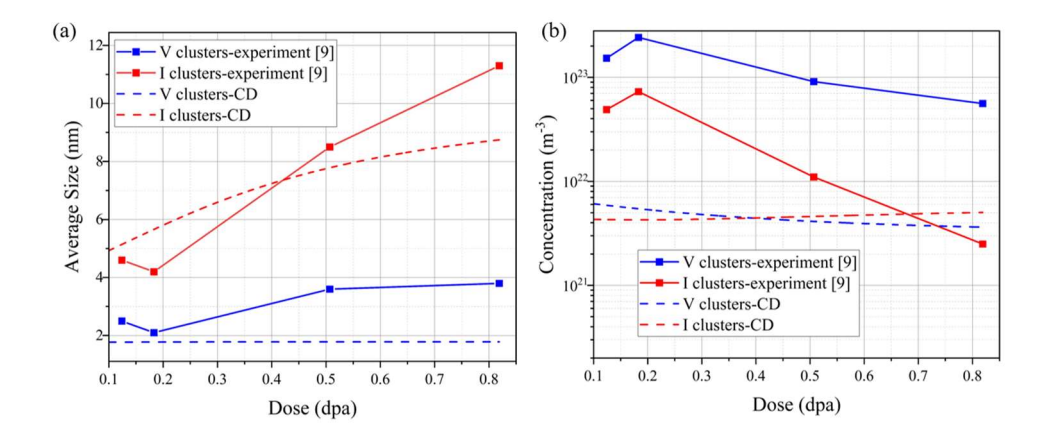


FIG. 4. The comparison between the experiment and simulation results for the average size and total concentration of visible clusters at 900 °C for polycrystalline W. The solid line represents the experimental data, while the dashed line denotes the experimental results: (a) Average size and (b) Total concentration.

We also performed similar simulations at 800 °C, and the results are shown in Fig. 5. In the experiment, the variations in defect size and concentration with dose exhibit similar trends between 800 °C and 900 °C. However, our simulation results show an overall decreasing trend in the average size of I clusters—a pattern that is completely opposite to the concentration trend observed at 900 °C. Moreover, the concentration at 800 °C is higher than that at 900 °C and demonstrates an increasing trend with dose.

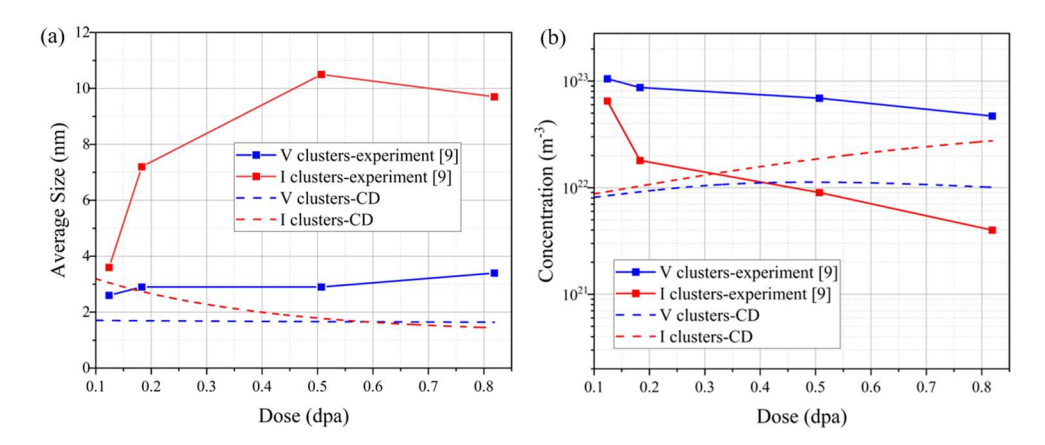


FIG. 5. The comparison between the experiment and simulation results for the average size and total concentration of visible clusters at 800 °C for polycrystalline W.

### 3.3. Analysis of discrepancies between experiment and simulation

The simulated defect concentrations for both single-crystal and polycrystalline W are consistently approximately one order of magnitude lower than the experimental values. A direct cause of this discrepancy may be an underestimation of the recombination rate between I and V clusters. This deviation is likely related to inaccuracies in cluster migration coefficients and limitations inherent in the rate theory itself. Further refinement of the rate theory may be necessary to achieve closer agreement with experimental data.

Furthermore, regarding the relationship between concentration and irradiation dose, both single-crystal and polycrystalline simulations show a clear saturation trend in cluster concentration with increasing dose—a phenomenon also observed in some ion irradiation experiments [32]. However, this saturation behaviour is not reflected in the experimental data for polycrystalline W; instead, the experimental defect concentration decreases with dose. We speculate that this difference may be attributed to transmutation-induced precipitates, whose formation is promoted at high doses by the increasing concentration of transmutation elements. Microstructural characterization by M. Klimenkov et al. [9] also clearly revealed the aggregation of transmutation elements Re

and Os. The apparent decrease in dislocation loops (I clusters) after 0.5 dpa may have been caused by the absorption of highly mobile dislocation loops at these transmutation-induced clusters, which act as efficient sinks.

For the decrease in dislocation loop size with dose at 800 °C, a trend opposite to that observed at 900 °C, we propose that the increased mobility of I clusters at higher temperatures may lead to enhanced absorption of small clusters by sinks such as V clusters, grain boundaries, and dislocation lines. This process significantly reduces the concentration of clusters available to grow into larger loops, resulting in a trend opposite to that observed experimentally. This discrepancy highlights the need for further optimization of the sink strength term and reaction rate parameters in the model.

### 4. CONCLUSIONS

This study employs a CD model to simulate neutron irradiation experiments on single-crystal and polycrystalline W in the BR2 reactor. The simulation results show general agreement with experimental observations. A detailed comparison was carried out regarding the average size and concentration of defect clusters between simulated and experimental data. Furthermore, possible origins of the observed discrepancies are discussed. A preliminary summary of the conclusions is as follows:

- 1. For high-dose neutron irradiation simulation (>0.1 dpa), the defect concentration in single-crystal W tends to saturate. Specifically, the concentration of I clusters decreases with increasing temperature, whereas the concentration of V clusters increases with temperature, accompanied by a growth in their average size.
- 2. For the irradiation simulation of polycrystalline W, the defect concentration still exhibits a saturation tendency. At 900°C, the size of I clusters increases with the irradiation dose. However, at 800°C, the model predicts a decreasing trend, which contradicts the experimental observations.
- 3. Key discrepancies with experiments include an order-of-magnitude lower defect concentration and inaccurate size evolution of V clusters and I clusters at  $800^{\circ}$ C, potentially due to simplifications regarding transmutation products and migration rates.

Therefore, further model improvements are necessary and will likely focus on more accurate cluster migration rates, the influence of transmutation-induced precipitates and impurities, as well as more precise rate equations to enhance predictive accuracy.

# **ACKNOWLEDGEMENTS**

This work is supported by the National Natural Science Foundation of China (Grant No. U2267208 and Grant No. 12305225).

# REFERENCES

- [1] RIETH, M., DOERNER, R., HASEGAWA, A., UEDA, Y., WIRTZ, M., Behavior of tungsten under irradiation and plasma interaction, Journal of Nuclear Materials **519** (2019) 334.
- [2] ASAKURA, N. et al., Recent progress of plasma exhaust concepts and divertor designs for tokamak DEMO reactors, Nuclear Materials and Energy **35** (2023) 101446.
- [3] HU, X., Recent progress in experimental investigation of neutron irradiation response of tungsten, Journal of Nuclear Materials **568** (2022) 153856.
- [4] TERENTYEV, D. et al., Recent progress in the assessment of irradiation effects for in-vessel fusion materials: tungsten and copper alloys, Nucl. Fusion **62** 2 (2022) 026045.
- [5] MARIAN, J. et al., Recent advances in modeling and simulation of the exposure and response of tungsten to fusion energy conditions, Nucl. Fusion **57** 9 (2017) 092008.
- [6] KLIMENKOV, M. et al., Effect of neutron irradiation on the microstructure of tungsten, Nuclear Materials and Energy **9** (2016) 480.
- [7] FUKUDA, M., TANNO, T., NOGAMI, S., HASEGAWA, A., Effects of Re Content and Fabrication Process on Microstructural Changes and Hardening in Neutron Irradiated Tungsten, Materials Transactions **53** 12 (2012) 2145.

- [8] TANNO, T. et al., Effects of Transmutation Elements on Neutron Irradiation Hardening of Tungsten, Materials Transactions 48 9 (2007) 2399.
- [9] KLIMENKOV, M. et al., Influence of transmutation-induced Re/Os content on defect evolution in neutron-irradiated W, Journal of Nuclear Materials **592** (2024) 154950.
- [10] HU, X. et al., Irradiation hardening of pure tungsten exposed to neutron irradiation, Journal of Nuclear Materials **480** (2016) 235.
- [11] KOYANAGI, T. et al., Microstructural evolution of pure tungsten neutron irradiated with a mixed energy spectrum, Journal of Nuclear Materials **490** (2017) 66.
- [12] DUBINKO, A. et al., Microstructure and hardening induced by neutron irradiation in single crystal, ITER specification and cold rolled tungsten, International Journal of Refractory Metals and Hard Materials **98** (2021) 105522.
- [13] TANNO, T., FUKUDA, M., NOGAMI, S., HASEGAWA, A., Microstructure Development in Neutron Irradiated Tungsten Alloys, Materials Transactions **52** 7 (2011) 1447.
- [14] FUKUDA, M. et al., Neutron energy spectrum influence on irradiation hardening and microstructural development of tungsten, Journal of Nuclear Materials **479** (2016) 249.
- [15] HASEGAWA, A., FUKUDA, M., YABUUCHI, K., NOGAMI, S., Neutron irradiation effects on the microstructural development of tungsten and tungsten alloys, Journal of Nuclear Materials **471** (2016) 175.
- [16] HU, X. et al., Transmutation-induced precipitation in tungsten irradiated with a mixed energy neutron spectrum, Acta Materialia 165 (2019) 51.
- [17] LI, Y.G. et al., A Cluster Dynamics Model For Accumulation Of Helium In Tungsten Under Helium Ions And Neutron Irradiation, Commun. comput. phys. 11 5 (2012) 1547.
- [18] MANNHEIM, A., VAN DOMMELEN, J.A.W., GEERS, M.G.D., Modelling recrystallization and grain growth of tungsten induced by neutron displacement defects, Mechanics of Materials 123 (2018) 43.
- [19] ZHANG, G.-S. et al., Simulation of neutron irradiation-induced recrystallization of tungsten, Acta Phys. Sin. **72** 16 (2023) 162801.
- [20] DUNN, A.Y., CAPOLUNGO, L., MARTINEZ, E., CHERKAOUI, M., Spatially resolved stochastic cluster dynamics for radiation damage evolution in nanostructured metals, Journal of Nuclear Materials **443** 1–3 (2013) 128.
- [21] MOHAMED, S. et al., Investigation of Microstructural Evolution of Irradiation-Induced Defects in Tungsten: An Experimental-Numerical Approach, (2024).
- [22] GILBERT, M.R., SUBLET, J.-Ch., Differential dpa calculations with SPECTRA-PKA, Journal of Nuclear Materials 504 (2018) 101.
- [23] GILBERT, M.R., MARIAN, J., SUBLET, J.-Ch., Energy spectra of primary knock-on atoms under neutron irradiation, Journal of Nuclear Materials **467** (2015) 121.
- [24] SETYAWAN, W. et al., Displacement cascades and defects annealing in tungsten, Part I: Defect database from molecular dynamics simulations, Journal of Nuclear Materials **462** (2015) 329.
- [25] OUDE VRIELINK, M.A., SHAH, V., VAN DOMMELEN, J.A.W., GEERS, M.G.D., Modelling the brittle-to-ductile transition of high-purity tungsten under neutron irradiation, Journal of Nuclear Materials **554** (2021) 153068.
- [26] SAND, A.E. et al., Cascade fragmentation: deviation from power law in primary radiation damage, Materials Research Letters 5 5 (2017) 357.
- [27] YI, X. et al., Direct observation of size scaling and elastic interaction between nano-scale defects in collision cascades, EPL **110** 3 (2015) 36001.
- [28] CASTIN, N. et al., On the onset of void swelling in pure tungsten under neutron irradiation: An object kinetic Monte Carlo approach, Journal of Nuclear Materials **493** (2017) 280.
- [29] MALERBA, L., BECQUART, C.S., DOMAIN, C., Object kinetic Monte Carlo study of sink strengths, Journal of Nuclear Materials 360 2 (2007) 159.
- [30] HINDMARSH, A.C. et al., SUNDIALS: Suite of nonlinear and differential/algebraic equation solvers, ACM Trans. Math. Softw. **31** 3 (2005) 363.
- [31] GARDNER, D.J., REYNOLDS, D.R., WOODWARD, C.S., BALOS, C.J., Enabling New Flexibility in the SUNDIALS Suite of Nonlinear and Differential/Algebraic Equation Solvers, ACM Trans. Math. Softw. **48** 3 (2022) 1.
- [32] CUI, S. et al., Thermal conductivity degradation and recovery in ion beam damaged tungsten at different temperature, Journal of Nuclear Materials **511** (2018) 141.